Title
Advancing SnO2–Based Water Dissociation Catalysis in Bipolar-Membrane Water Electrolyzers

Journal
ACS Energy Letters, 10(4)

ISSN
2380-8195

Authors
Han, Sanghwi
Sasmal, Sayantan
Shen, Meikun
et al.

Publication Date
2025-04-11

DOI
10.1021/acsenergylett.5c00309

Advancing SnO_2-Based Water Dissociation Catalysis in Bipolar-Membrane Water Electrolyzers

Sanghwi Han[a,b], Sayantan Sasmal[a], Meikun Shen[c], Yifan Wu[d], Olivia T. Vulpin[a], Shujin Hou[d], Sungjun Kim[e], Jang Yong Lee[f], Jeyong Yoon*[b], Shannon W. Boettcher*[a,d,g]

[a]*Department of Chemistry and Biochemistry, Oregon Center for Electrochemistry, University of Oregon, Eugene, Oregon 97403, United States.*

[b]*School of Chemical and Biological Engineering, Institute of Chemical Processes, Seoul National University, Seoul 08826, Republic of Korea.*

[c]*Department of Chemistry and Geosciences, Jacksonville State University, Alabama 36265, United States*

[d]*Department of Chemical & Biomolecular Engineering and Department of Chemistry, University of California, Berkeley, California 94720, United States.*

[e]*Hydrogen Energy Research Center, Korea Research Institute of Chemical Technology (KRICT), Daejeon 34114, Republic of Korea*

[f]*Department of Chemical Engineering, Konkuk University, Seoul 05029, Republic of Korea*

[g]*Energy Storage and Distributed Resources Division, Lawrence Berkeley National Laboratory, Berkeley, California 94720, United States*

* Email: boettcher@berkeley.edu; jeyong@snu.ac.kr

ABSTRACT

Advancing water dissociation (WD) catalysis is important for bipolar membrane (BPM) technology for energy-conversion systems. We report a one-step strategy for synthesizing SnO_2-based WD catalysts directly on a cation-conducting membrane, which is straightforward, fast, and scalable, while exhibiting record-high WD performance. Electrochemical and material analyses show that the thickness and heterogeneity of the SnO_2 layer are the primary factors governing ionic transport in the SnO_2 WD catalyst layer and influencing WD performance. At optimal deposition conditions, the SnO_2 catalysed BPM electrolyzer has a low total cell voltage at 1 A cm^{-2} of 1.93 V and a WD overpotential (η_{wd}) of 41 ± 7 mV. These performance metrics were maintained across various 1.5 cm × 1.5 cm sections upon the fabrication of a 100 cm^2 BPM. This BPM electrolyzer, operating with pure-water feed in a membrane-electrode-assembly architecture, was durable, with a degradation rate of 0.5 mV h^{-1} over 100 h at 1.0 A cm^{-2} and the η_{wd} increase of 0.27 mV h^{-1}.

MAIN TEXT

Bipolar membranes (BPMs) are a class of ion-conductive membranes, composed (typically) of a polymeric cation-exchange layer (CEL) and anion-exchange layer (AEL) and often incorporate an intermediate catalyst layer between them. The CEL contains fixed negatively charged groups, enabling the selective conduction of cations, whereas the AEL contains fixed positively charged groups, facilitating the selective transport of anions.[1–5] In "reverse bias", BPMs drive water dissociation (WD, $H_2O \rightarrow H^+ + OH^-$) and separate the incipient H^+ and OH^- within the CEL/AEL junction to carry ion current and allow the maintenance of a stable, steady-state pH gradient between the catholyte/cathode and anolyte/anode. This capability enables their use in ion-separation systems for electrodialysis,[6] capacitive deionization,[7,8] and acid-base synthesis[9] as well as in energy-conversion technologies like water[10–14] and CO_2[15–17] electrolysis, fuel cells,[18] and carbon-capture systems.[19,20] However, the BPMs usually have much higher resistance to ion transport compared to single-membrane systems, with the kinetics of WD at the bipolar junction often limiting. This limitation has historically hindered the development and commercialization of energy-conversion technologies leveraging BPMs as cell components.

Building on the early understanding of the mechanism of WD on heterogeneous surfaces in the BPM, there has been substantial recent progress in catalyst development. Many catalysts, including metal oxides,[3,10,13,21] metal sulfide,[22] and graphene oxide,[23,24] have been developed to reduce the voltage loss or overpotential for WD (η_{wd}). The coverage or thickness of the WD catalyst layer is known to affect η_{wd}, with nominally full coverage optimal for graphene oxide nanoflakes and the ideal thickness for metal-oxide catalysts apparently determined by their electronic properties.[21,23,25] For semiconducting WD catalysts such as TiO_2, the optimal loading and thickness range is 10–30 μg cm^{-2} and 200–600 nm, respectively, while electronic conductors (e.g., F:SnO_x, IrO_x, and Pt) have high performance with higher loading and a wider optimal range.[13] The acid-base properties of metal oxides, indicated by their pH of zero charge (PZC), also play a role, with bilayers of basic PZC oxides adjacent to the AEL and acidic PZC oxides near the CEL outperforming single-component WD catalyst layers.[3] Temperature-dependent measurements of the WD kinetics demonstrate that applied voltage accelerates WD by enhancing the kinetic pre-factor rather than reducing activation energy.[1,14] A recent study suggested that η_{wd} of metal-oxide catalysts is governed by minimally three descriptors—electrical conductivity, microscopic surface area, and nominal surface-hydroxyl coverage—leading to the development of a 3-nm SnO_2 catalyst exhibiting a low η_{wd} of ~100 mV at 1 A

cm^{-2}.[25] Based on these experiments, we proposed a mechanism in which oxide-based WD catalysts electronically polarize within the BPM junction to a degree depending on their electrical conductivity (or dielectric constant). This local electronic polarization is thought to organize the interfacial water molecules, reducing their entropy, and increasing the probability of water serving as a proton donor to the oxide surface on one side of the nanoparticle catalyst while serving as a proton acceptor at the other, with protons shuttling across the particle surface at steady state. This physical picture explains why SnO_2 nanoparticles synthesized at low temperatures having high concentrations of surface hydroxyl groups, high surface area, and reasonably high electronic conductivities are particularly good at dissociating water in the BPM. Despite recent advances, further lowering of the BPM losses through advanced WD catalysts that are easy to produce, reproducible, and scalable is useful to drive advanced BPM technology, for example BPM-based electrolyzers.

Here, we present a facile and scalable one-step approach for directly synthesizing a SnO_2 WD catalyst onto the Nafion membrane. By controlling catalyst loading, thickness, and surface properties, we found that 70 μg cm^{-2} and ~400 nm in thickness as the optimal parameters. We discovered that WD performance improves when SnO_2 particles exhibit partial aggregation and uneven thickness, which we hypothesize promotes efficient ionic transport. The directly coated SnO_2 WD catalyst enables BPM pure water electrolyzers to operate at 1 A cm^{-2} at 1.93 ± 0.02 V and a η_{wd} of 41 ± 7 mV. These performance metrics were maintained across different 1.5 cm × 1.5 cm sections when a 100 cm^2 BPM was fabricated. The new BPM electrolyzer operates with a degradation rate of ~0.5 mV h^{-1} for 100 h at 1.0 A cm^{-2} and a 27 mV increase in η_{wd}, consistent with the known degradation of alkaline anodes.[26–28]

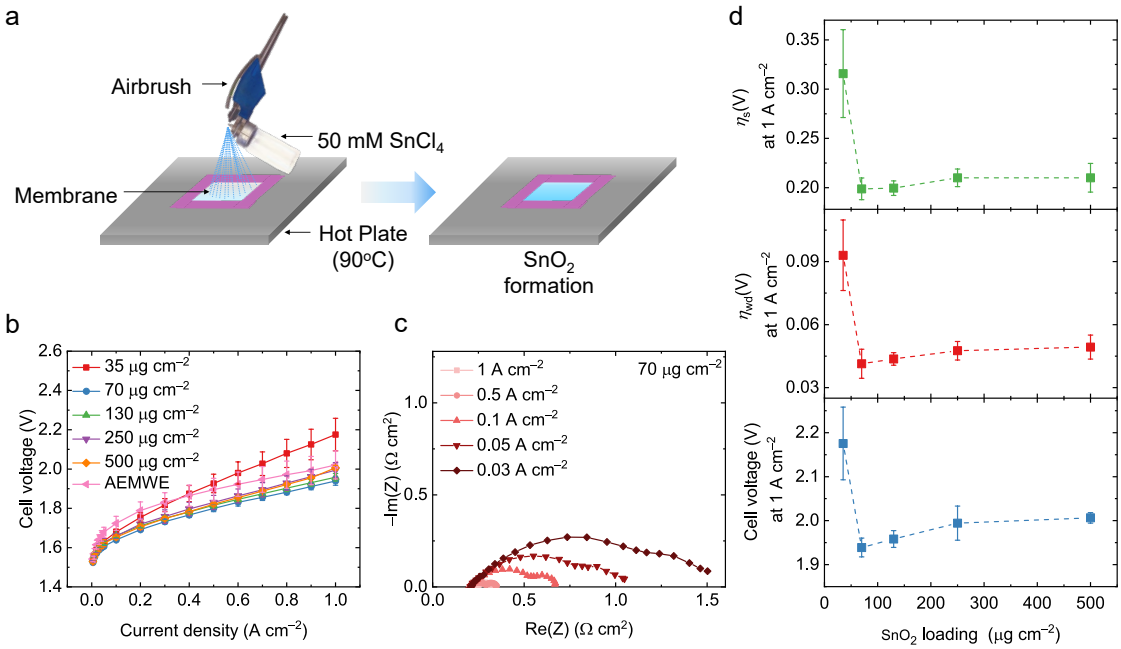

Figure 1. Directly coated SnO_2 WD catalyst for BPM electrolyzer. (a) Schematic of directly coated SnO_2 WD catalyst on a Nafion membrane. (b) Polarization curves of BPM electrolyzers with different loadings of SnO_2 WD catalysts. (c) Nyquist plots of BPM electrolyzers at various current densities with a SnO_2 WD catalyst of 70 μg cm^{-2}. (d) Overpotentials and cell voltage of BPM electrolyzers with different loadings of SnO_2 WD catalysts. Error bars indicate standard errors obtained from three independent replicates.

Effects of the loading and thickness of SnO_2 WD catalyst on BPM electrolyzer. The WD catalyst layer was nominally SnO_2 synthesized by spraying $SnCl_4$ solution onto the Nafion membrane heated to 90 °C on a hot plate (**Figure 1a**) via a reaction $SnCl_4 + 2H_2O \rightarrow 4HCl + SnO_2$. The formation of SnO_2 was found through grazing-incidence X-ray diffraction (GIXRD) and Raman spectroscopy (**Figure S1**). We evaluated the performance of the SnO_2 WD catalysts within pure water-fed BPM electrolyzers using a membrane-electrode assembly (MEA). Paired with the catalyst-coated Nafion was an HQPC-TMA AEL membrane, which demonstrated high performance at elevated temperatures (~80 °C).[29] To compare different WD catalysts, the Pt hydrogen-evolution-reaction (HER) catalyst, spray-coated Co_3O_4 oxygen-evolution-reaction (OER) catalyst, assembly methods, temperature, etc. are all kept identical (see methods section). We first assessed the performance of the SnO_2 WD catalysts by adjusting their mass loadings. The BPM electrolyzer achieved optimal performance at a SnO_2 loading of 70 μg cm^{-2}, operating at 1 A cm^{-2} with a total cell voltage of 1.93 ± 0.02 V (**Figure 1b**). Note that the system without a WD catalyst could not sustain operation at 1 A cm^{-2} for more than 10 min, as the cell voltage surpassed 10 V, preventing further evaluation. We determined the series resistance (R_s), WD resistance (R_{wd}), and charge transfer resistance (R_{ct}) at each current density through

electrochemical impedance spectroscopy (EIS) equivalent circuit analysis (**Figures 1c, S2,** and **S3**) and integrated these values over current to calculate the overpotentials at 1 A cm^{-2} (**Figure S4**). As observed in our previous studies, the Nyquist plot displayed three semicircles.[13,14] The first semicircle showed minimal dependence on current density, consistent with it being associated with the resistance for WD. The second and third semicircles are attributed to charge transfer (CT) processes at the two electrodes being strongly dependent on the total current/voltage, and largely independent of the WD catalyst layer. At the lower levels of catalyst loading such as for 35 μg cm^{-2} (**Figure S3b**), R_{wd} decreases as current density increases, consistent with previous studies.[13] This is consistent with the physical picture that insufficient WD catalyst requires a higher local electric field to drive WD. The η_{wd} values obtained from EIS analysis aligned with those measured via membrane-potential sensing using two reference electrodes (**Figure S5**).[13,14,25] All subsequent η_{wd} measurements reported are derived from fitting the EIS data as a function of current.

Interestingly, we found that the overall cell-voltage trend closely mirrored that of the overpotentials for series-resistance ($\eta_s = I{\cdot}R_s$) and water dissociation $\eta_{wd} = I{\cdot}R_{wd}$ (**Figure 1d**) where the resistances are derived from the impedance analysis. That is, the WD catalyst apparently influences not only the derived η_{wd}, but also the derived η_s. While the difference in η_{wd} at 1.0 A cm^{-2} between the optimal (70 μg cm^{-2}) and lowest points (35 μg cm^{-2}) is approximately 50 mV, the difference in η_s is around 110 mV, indicating that across these different formulations of active WD catalysts, η_s apparently has a more pronounced impact on overall cell performance.

The variations in R_s may stem from differences in ionic transport within the WD catalyst layer.[13] To compare ionic conductivity, we measured electrolyzer polarization curves and performed a linear fit of the high current density (500–1000 mA cm^{-2}) region to determine the differential resistance $\left.\frac{dV}{dI}\right|_{I\to\infty} = R_{slope}$ (**Figure S6**). At these high currents, R_{slope} is primarily governed by ohmic losses due to electronic and ionic transport, as the rates of both HER and OER generally increase exponentially with overpotential. Because there is no electronic current flowing in the WD-catalyst layer, the differences in R_{slope} must be due to ionic processes within the WD layer.

The R_{slope} shows a trend similar to R_s, measured by the high-frequency impedance, with a difference of ~0.2 Ω cm^2 between the optimal and lowest points. Given that the R_{wd} difference between these points is only about 0.03 Ω cm^2 at 1.0 A cm^{-2} (**Figure S3b**), it is evident that variations in ionic-transport resistance probably dominate performance differences.

In our previous study, we reported that in environments where R_{wd} varies by ~5 Ω cm^2 according to the WD catalysts, ionic transport resistance fluctuates only 0.1–0.2 Ω cm^2, rendering ionic transport relatively insignificant.[13] However, in the present system, the minimal difference in R_{wd} of ~0.03 Ω cm^2 amplifies the importance of relatively small differences in ionic transport resistance on performance.

We calculated a term defined here as the remaining overpotential (η_{rest}) by subtracting η_{wd}, η_s, and kinetic overpotential (η_{kin}) from total overpotential (**Figure S7**). The term η_{rest} is often attributed to mass-transport in water electrolysis systems.[30–33] In contrast to fuel cells, where gas transport into porous electrodes plays a critical role, gas bubbles in water electrolysis are more easily expelled at high flow rates (~125 mL min^{-1} in our system). To ensure this is the case here, the flow rate was varied from 1 to 125 mL min^{-1}. We found no significant performance difference up to 1 A cm^{-2} (**Figure S8**). Consequently, we hypothesize this resistance/overpotential is primarily attributed to the electrocatalyst layers (anode and cathode), which function as a network of resistors and capacitors, with this resistance not being reflected in the R_s measurement. In-plane conductivities of the SnO_2-coated Nafion were measured, but a lack of correlation with system performance suggests that ionic transport critical for BPM water electrolysis predominantly occurs through-plane, rather than in-plane (**Figure S9**).

A comparison between optimal BPM and control AEM electrolyzers revealed higher performance for the BPMWE. While the BPM exhibited slightly higher η_s of 0.1 ± 0.01 V, likely associated with the additional CEM layer and ionic resistance in the WD catalyst layer, as well as the η_{wd} of 0.04 V, BPMWE achieved a lower cell voltage due to reduced η_{kin} of 0.18 ± 0.02 V (**Figure S10**). This enhanced kinetics is attributed to the much higher HER activity of the Pt cathode under strong-acid local-pH conditions present in the BPM system, compared to alkaline conditions where the WD reaction must be driven on the cathode catalyst surface to form metal-hydride intermediates.[34] Overall, the BPM electrolyzer incurs a ~100 mV η_s loss but gains ~180 mV in η_{kin} compared to anion exchange membrane water electrolyzer (AEMWE), requiring a η_{wd} below 80 mV to outperform the AEMWE. Our results confirm that the superior performance of the SnO_2 WD catalyst enables the BPM electrolyzer to surpass AEMWE in this particular application. Practically, a commercial proton exchange membrane water electrolyzer (PEMWE) might operate at ~1.7 V at 2 A cm^{-2}, resulting in a total overpotential of ~500 mV. Given this, if the WD overpotential exceeds 100 mV at 2 A cm^{-2}, it would add 20% to the total overpotential, which is probably not acceptable. Therefore, for water-electrolysis applications, a WD overpotential in the range of tens of millivolts at relevant currents of near 2 A cm^{-2} is

probably required. In contrast, for BPM electrodialysis (BPMED), the current level of η_{wd} is probably satisfactory. For instance, in our recent study, BPMED operated at 0.5 A cm^{-2} with a total voltage of approximately 5 V, where the WD overpotential was around 300 mV for the particularly membrane tested, accounting for only 6% of the total overpotential.[35] Because commercial BPMED systems typically operate at ~0.1 A cm^{-2}, η_{wd} of our best membranes are expected to contribute negligible to the overall voltage. The current WD performance is thus likely suitable even for future high-current BPMED stacks.

AEMWE instead of PEMWE was chosen as a baseline to compare with as both AEMWE and BPMWE share a common alkaline ionomer anode. This alkaline ionomer anode enables the use of the non-Ir electrocatalyst, but the ionomer stability remains a major issue.[36,37] Because of the durability and performance issues associated with the anode, neither BPMWE nor AEMWE can compete practically with PEMWE today when pure-water electrolyte is desired.

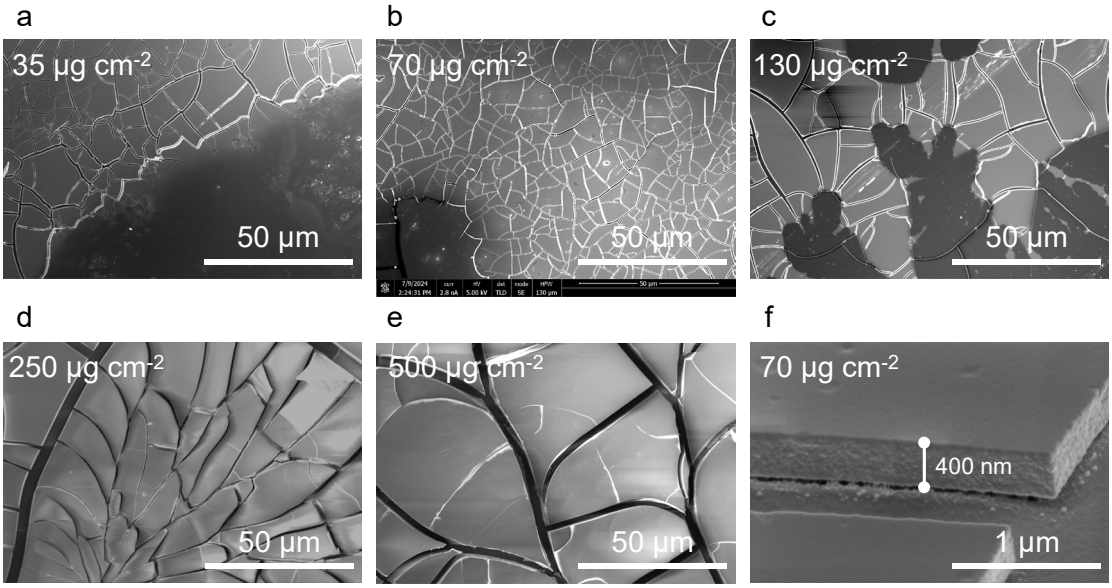

Figure 2. Surface morphologies of SnO_2 WD catalysts. SEM images of SnO_2 WD catalyst with (a) 35, (b) 70, (c) 130, (d) 250, and (e) 500 μg cm^{-2}, which were fabricated at 90 °C. (f) Cross-sectional SEM image of SnO_2 WD catalyst with 70 μg cm^{-2}.

The SnO_2 layer directly coated on the Nafion membrane forms a cracked film structure (**Figure 2**). Optical microscope images (**Figure S15**) and Raman analysis (**Figure S1c**) reveal cracks in all SnO_2 catalyst layers, indicating that the cracks shown in scanning electron microscopy (SEM) images do not originate from SEM vacuum conditions. At low loading levels, the SnO_2 layer exhibits partial aggregation, allowing F in Nafion to be detected via energy dispersive spectroscopy (EDS) analysis (**Figure S11**); however, at higher loading levels, only the SnO_2

layer is visible (**Figure S12**). In both cases, EDS analysis reveals an Sn-to-O ratio of approximately 1:2 (**Table S1**). Cross-sectional SEM images reveal that the catalyst layer thickness increases from approximately 100 to 2,200 nm as the loading rises from 35 to 500 μg cm^{-2} (**Figure S13**). In the 70 μg cm^{-2} sample, the catalyst layer exhibits uneven thickness, ranging from approximately 100 nm (**Figure S13b**) in some areas to 400 nm (**Figure 2f**). AFM analysis also reveals that low-loading catalysts exhibit a non-uniform thickness ranging from tens to hundreds of nanometers, whereas high-loading catalysts form a consistently thick layer (**Figure S14**). X-ray photoelectron spectroscopy (XPS) analysis further indicates that as the catalyst loading increases, the F peaks become less detectable at loadings > 130 μg cm^{-2} owing to the thick SnO_2 layer (**Figure S16**). The binding energy of Sn 3d remained largely unchanged across different loading amounts. Collectively, the physical properties of the SnO_2 layer, such as thickness and uniformity, vary with the loading amount, while its chemical state remains unaffected. The results suggest that the surface morphology of the catalyst has a substantial impact on WD performance, with efficient ionic transport requiring both optimal thickness (~400 nm) and may also benefit from thickness/structural non-uniformity.

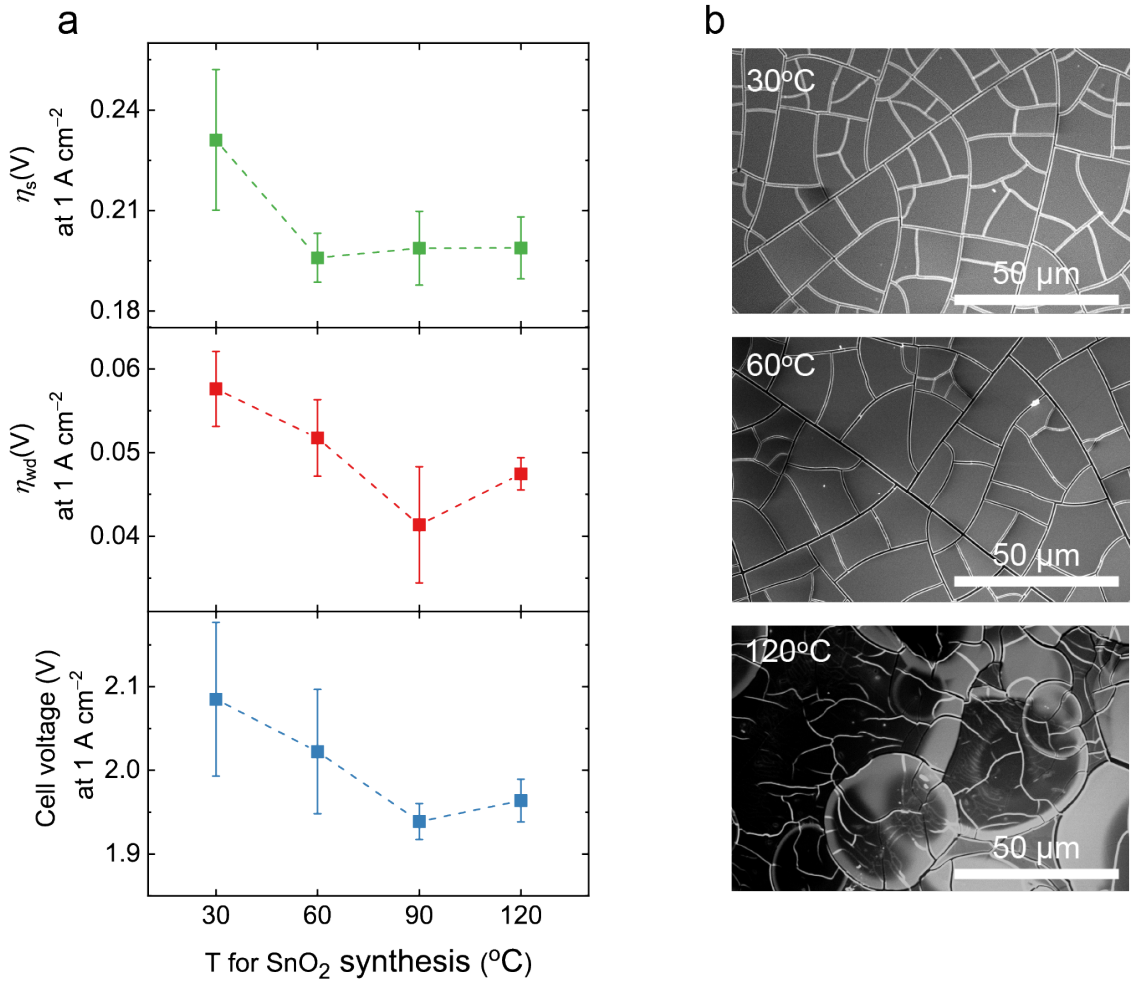

Figure 3. Temperature effect on SnO_2 WD catalyst formation. (a) Performance of BPM electrolyzers with SnO_2 WD catalysts fabricated with various temperatures. (b) SEM images of SnO_2 WD catalyst fabricated at 30, 60, and 120 ºC. Error bars indicate standard errors obtained from three or more independent replicates.

Tuning morphologies of the SnO_2 layer. To study the relationship between the physical properties of the SnO_2 layer and WD performance, we modified the morphology by varying the synthesis temperature of SnO_2 while fixing the loading amount at 70 μg cm^{-2}. The hot-plate temperature for spray coating was varied at 30, 60, 90, and 120 ºC, with these adjustments expected to impact the nucleation and growth processes of SnO_2 particles.[38] The SnO_2 synthesis temperature impacts cell performance, η_{wd}, and η_s in the BPM electrolyzers, with optimal performance observed at 90 °C (**Figures 3a** and **S17**). Consistent with the observed trend in loading, the cell voltage and η_s strongly correlate with ionic resistance (**Figure S18**). SEM images reveal that a thin, homogeneous layer of approximately 90 nm is formed at 30 ºC, potentially impeding efficient ionic transport or not resulting in the required crystalline oxide phases for WD (**Figures 3b** and **S19**). Given a bulk SnO_2 density of 7 g cm^{-3}, a WD catalyst layer thickness at 70 μg cm^{-2} would be ~100 nm if the SnO2 was fully dense. This is similar to the thickness found for the WD catalyst film synthesized at 30 °C. In contrast, synthesis at higher temperatures results in a more uneven surface structure and larger average thickness, indicating increased porosity. This phenomenon can be attributed to the rapid synthesis of SnO_2 at higher temperatures, accompanied by active water evaporation driving non-uniformity and porosity. In contrast, at lower temperatures, the slow reaction kinetics facilitate the formation of the uniform and thin layer. SEM and AFM analyses demonstrate that the thickness of the SnO_2 layer increases with rising synthesis temperature, with the sample synthesized at 120 ºC exhibiting a thickness of approximately 400 nm (**Figures S19** and **S20**). The sample synthesized at 120 ºC exhibits a similar catalyst structure and thickness to the 90 ºC sample; however, it demonstrates lower WD performance in the BPM electrolyzer. A temperature of 120 ºC may trigger the glass transition of Nafion and destabilize the structure of the polymer due to the relaxation of its polymer chains.[39,40]

Collectively, our findings suggest that physical properties, such as thickness and uniformity, have a significant impact on WD performance. Through systematic adjustment of the loading amount, we identified that a thickness of approximately 400 nm yields the optimal WD performance in the BPM electrolyzer for the directly coated SnO_2 catalyst. The uniformity of the catalyst layer also varied across the different samples tested. The sample synthesized at

30 °C is the most uniform and despite having a thickness similar to the 60 °C sample (**Figures S19** and **S20**), exhibited significantly lower WD performance (**Figure 3a**). However, the lower temperature is expected to also affect the catalyst formation and therefore deconvoluting the effects of thickness, uniformity, and chemistry of the WD layer is not fully possible from this study.

In a prior study, we pre-synthesized 3-nm SnO_2 nanoparticles for the WD catalyst, demonstrating high WD performance.[25] This superior efficiency was attributed to relatively high electrical conductivity and abundant hydroxyl coverage persevered on the particle surface by avoiding a calcination step.

The primary distinction between 3-nm SnO_2 and directly coated SnO_2 in this study lies in their preparation methods. In this study, the SnO_2 layer was formed *in situ* on the Nafion membrane in a single step, whereas the 3-nm SnO_2 particles were synthesized in an aqueous solution, filtered via centrifugation, dissolved in spray ink solution, and spray-coated on a membrane. For the 3-nm SnO_2 catalyzed BPM, a loading of 30 μg cm^{-2} was used, as determined to be optimal in the previous study. For the directly coated SnO_2, a loading amount of 70 μg cm^{-2} and a synthesis temperature of 90 ºC was used. The comparison between directly coated SnO_2 and 3-nm SnO_2 catalysts at different loading amounts was conducted because the optimal loading conditions differ for each catalyst and we aimed to compare the best performance for both.

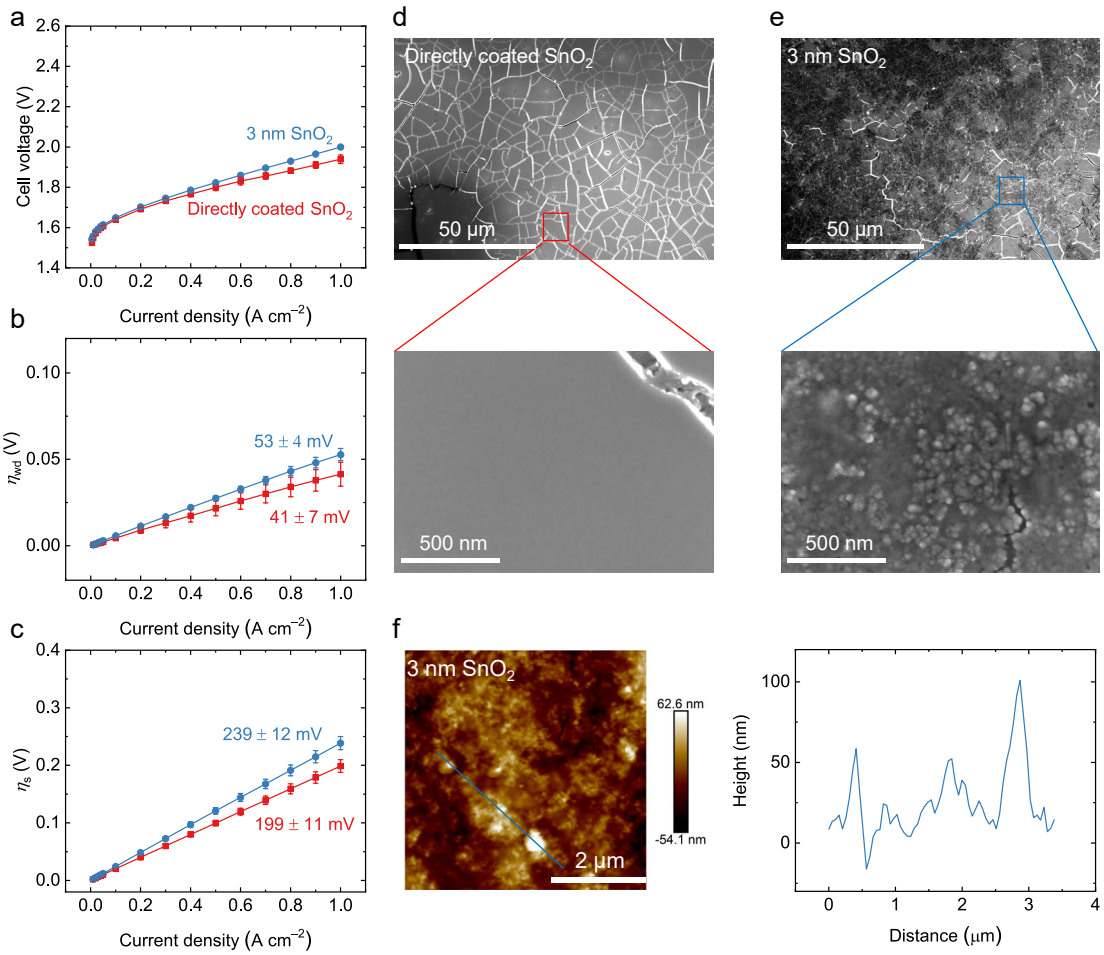

Figure 4. Comparison of directly coated SnO_2 and pre-synthesized 3-nm SnO_2 WD catalyst. (a) Polarization curves, (b) η_{wd} measurement, and (c) η_s measurement for directly coated SnO_2 and 3-nm SnO_2. SEN images of (d) directly coated SnO_2 and (e) 3-nm SnO_2. (f) AFM height and corresponding line-cut plots of 3-nm SnO_2. The blue line in (f) represents the measurement area. Error bars indicate standard errors obtained from three or more independent replicates.

In the BPM electrolyzer, the directly coated SnO_2 demonstrated an overpotential of approximately 50 mV lower at 1 A cm^{-2} compared to the 3-nm SnO_2 (**Figure 4a**). This reduction is attributed to a decrease in η_{wd} by around 12 mV (**Figure 4b**) and η_s by approximately 40 mV (**Figure 4c**). Thus, the performance disparity is primarily attributed to differences in η_s, resulting from differences in ionic resistances, given the identical cell design and electrodes/catalysts (**Figures S21a–b**).

SEM images revealed a distinct difference in the morphology of the two WD catalysts. The directly coated SnO_2 forms an uneven cracked SnO_2 layer, with no discernible particles even under magnification (**Figure 4d**). In contrast, the 3-nm SnO_2 exhibits a rough surface morphology, consisting of clusters of aggregated nanoparticles (**Figure 4e**). The rough surface

characteristics of the 3 nm SnO_2 were also found by AFM analysis (**Figure 4f**). AFM and cross-sectional SEM analyses reveal that the 3-nm SnO_2 possesses a thickness of approximately 100 nm (**Figure S22**). This suggests that the optimal thickness varies, likely due to differences in surface properties between the directly coated SnO_2 and the 3-nm SnO_2.

When the directly coated SnO_2 was removed from the Nafion, sonicated, and analyzed using transmission electron microscopy (TEM), particles approximately 3 nm in size were observed (**Figure S23**). The directly coated SnO_2 thus appears to consist of small particles that coalesce to form thin films. XPS analysis was performed on the 3-nm SnO_2 and directly-coated SnO_2 catalyst and no significant differences were observed in the Sn 3d and O 1s spectra (**Figure S24**). During the formation of the directly coated SnO_2 WD catalyst, the Lewis acidic $SnCl_4$ reacts with water, releasing HCl, and subsequently undergoes crosslinking and condensation reactions at the deposition temperatures, similar to those used for 3-nm SnO_2 formation, forming SnO_2 nanoparticle directly on the membrane. As both materials are formed through a similar environment, the similarity in chemical state is expected. However, due to the molecular size of the $SnCl_4$ precursor, the directly coated SnO_2 particles are likely more deeply embedded within the Nafion matrix, creating a more-intimate interface that may enhance local electrical field or other parameters that increase WD and ion-transport performance compared to 3-nm SnO_2. While the performance of the directly coated SnO_2 in terms of WD catalysis overpotential is excellent, perhaps more importantly is the simplicity of the process, compared to the 3-nm SnO_2 catalysts which must be synthesized and cleaned, the only requirement for the new process is to prepare a 50 mM $SnCl_4$ solution and spray it onto a large-area cation-exchange membrane.

Potential scale-up of the SnO_2 WD catalyst. For commercial relevance, WD catalysts must demonstrate high performance, scalability, and durability. To assess the scalability of the WD catalyst layer synthesis and deposition approach, we fabricated a 100 cm^2 SnO_2-coated Nafion membrane using a spray coater (**Figure S25**). The SnO_2 WD catalyst was synthesized using the optimized loading of 70 μg cm^{-2} and synthesis temperature of 90 ºC. We extracted five 1.5 cm × 1.5 cm sections from the 100 cm^2 SnO_2-coated membrane and evaluated their performance in the BPM electrolyzers. All five sites had comparable η_{wd} and η_s, with the values falling within the error and aligning closely with the optimal reference data (**Figure S25)**. This result indicates the scalability of the developed SnO_2 WD catalyst to large areas.

We tested the durability of the directly coated SnO_2 BPM using a BPM electrolyzer, operating at a current density of 1.0 A cm^{-2}. When a spray-coated Co_3O_4 anode was used, the cell voltage rose from 1.9 V to 2.4 V within a few hours (**Figure S26**). Given the documented poor durability of spray-coated anode/ionomer catalyst layers in pure-water-fed anion-exchange-membrane water electrolyzers,[28,41–44] the observed increase in cell voltage is attributed to the degradation of the anode. When a bare stainless steel (SS) felt anode without a catalyst was employed, the initial performance was poor but after 20 h of operation, the performance surpassed that of the Co_3O_4 anode (**Figure S26**).

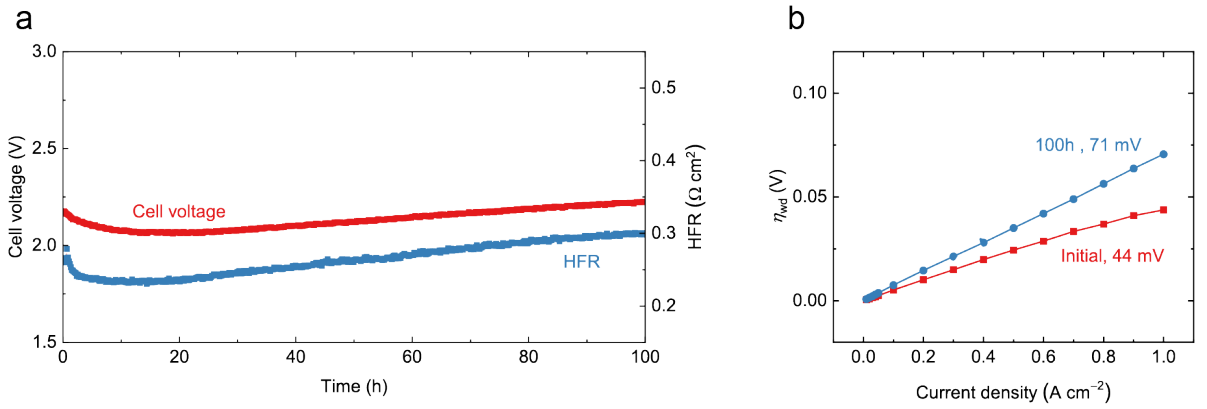

Figure 5. Durability of direct-coated SnO_2 WD catalyst. (a) Cell voltage and HFR traces at 1 A cm^{-2} for 100 h of operation. (b) Comparison of η_{wd} at 1 A cm^{-2} before and after 100 h of operation.

Accordingly, we pursued the parallel development of the OER catalyst to enhance its durability. We developed a simple electrodeposited Co-based catalyst (ED-Co) with higher durability via optimization of electrodeposition conditions and the HQPC-TMA ionomer top coating. Using the ED-Co anode, the SnO_2 WD catalyst underwent a 100 h durability test at 1.0 A cm^{-2} (**Figure 5a**). Over 100 h, the BPMWE system exhibited a degradation rate of approximately 0.5 mV h^{-1}. High-frequency resistance (HFR) analysis over the course of the test showed that variations in cell voltage correlate with changes in R_s, indicating that HFR significantly influences overall cell performance. After 100 h, the HFR increased by 0.03 Ω cm^2, corresponding to a potential increase of ~30 mV. Given that the voltage rose by ~50 mV during the same period, the increase in HFR appears to induce the majority of the change. EIS analysis shows an increase in η_{wd} of 27 mV after 100 h (**Figures 5b** and **S27**). These results indicate that the increases in η_s and η_{wd} are comparable, highlighting the importance of membrane development alongside WD catalysts for advancing BPM systems. Surface analysis of the WD catalyst after 100 h was hindered by strong adhesion between the AEL and CEL, likely due to prolonged exposure to high

temperature and pressure, which may have altered their physical properties and made separation challenging without causing mechanical damage. This new BPM electrolyzer system with the SnO_2 WD catalyst has demonstrated exceptional performance compared to previous studies (**Figure S28** and **Table S2**).

We recently reported a simple design for a BPMED test platform that enables the isolation of potential drops across individual membranes, allowing for the precise measurement of key parameters such as η_{wd} within the BPM system.[35] These measurements revealed that the overpotential trends of WD catalysts in BPMED closely resemble those observed in BPMWE when tested in reverse bias, likely because most of the co-ions are electrodialyzed out of the BPM junction. Therefore, the directly coated SnO_2 WD catalyst developed in this study is expected to be applicable to BPMED and other BPM systems where the membrane is in contact with solutions of soluble salt and not only pure water as is studied here. Additional work is merited to fully understand the difference in BPM response for electrodialysis, CO_2 reduction, and carbon-capture systems, and other electrochemical technologies.

In summary, we developed a straightforward and scalable one-step approach for directly synthesizing a SnO_2 WD catalyst on the Nafion membrane. The directly coated SnO_2 forms a cracked film on Nafion, with some partial agglomeration and non-uniform thickness. The optimal loading and thickness were found to be 70 μg cm^{-2} and ~400 nm, respectively. We verified that this trend persisted even after adjusting the synthesis temperature and modifying the surface structure. The directly coated SnO_2 WD catalyst layers enable BPM pure-water electrolyzers to operate at a current density of 1.0 A cm^{-2} with a cell voltage of 1.93 ± 0.02 V and a η_{wd} of 41 ± 7 mV, maintaining consistent performance even when scaled up to a 100 cm^2 surface area. This BPM electrolyzer was durably operated with a degradation rate of 0.5 mV h^{-1} at 1.0 A cm^{-2} and a 27 mV increase in η_{wd} over 100 h. Considering the simplicity, scalability, and high performance of this WD catalyst, this study is anticipated to apply to and contribute to the advancement of membrane and technology development efforts within the BPM field.

ASSOCIATED CONTENT

Supporting Information

The Supporting Information is available free of charge at http://pubs.acs.org.

Detailed experimental procedures for BPM Electrolyzer fabrication and measurements, membrane-potential sensing, preparation of WD catalysts, in-plane conductivity measurement, and materials characterization; additional results on electrochemical experiments, and material

characterization results including the Raman spectroscopy, SEM, EDS elemental mapping, AFM, XRD patterns, XPS, and TEM analyses.

AUTHOR INFORMATION

Corresponding Author

Shannon W. Boettcher − *Department of Chemical & Biomolecular Engineering and Department of Chemistry, University of California, Berkeley, California 94720, United States; Energy Storage and Distributed Resources Division, Lawrence Berkeley National Laboratory, Berkeley, California 94720, United States; Department of Chemistry and Biochemistry and Oregon Center for Electrochemistry, University of Oregon, Eugene, Oregon 97403, United States; orcid.org/ 0000-0001-8971-9123; Email: boettcher@berkeley.edu*

Jeyong Yoon − *School of Chemical and Biological Engineering, Institute of Chemical Processes, Seoul National University (SNU), Seoul 08826, Republic of Korea; orcid.org/ 0000-0003-4455-3670;* Email: jeyong@snu.ac.kr

Authors

Sanghwi Han − *Oregon Center for Electrochemistry, Department of Chemistry and Biochemistry, University of Oregon, Eugene, Oregon 97403, United States; School of Chemical and Biological Engineering, Institute of Chemical Processes, Seoul National University (SNU), Seoul 08826, Republic of Korea; orcid.org/ 0000-0002-0017-1550*

Sayantan Sasmal − *Oregon Center for Electrochemistry, Department of Chemistry and Biochemistry, University of Oregon, Eugene, Oregon 97403, United States*

Meikun Shen − *Department of Chemistry and Geosciences, Jacksonville State University, Alabama 36265, United States*

Yifan Wu − *Department of Chemical & Biomolecular Engineering and Department of Chemistry, University of California, Berkeley, California 94720, United States*

Olivia T. Vulpin − *Oregon Center for Electrochemistry, Department of Chemistry and Biochemistry, University of Oregon, Eugene, Oregon 97403, United States*

Shujin Hou − *Department of Chemical & Biomolecular Engineering and Department of Chemistry, University of California, Berkeley, California 94720, United States*

Sungjun Kim − *Hydrogen Energy Research Center, Korea Research Institute of Chemical Technology (KRICT), Daejeon 34114, Republic of Korea*

Jang Yong Lee − *Department of Chemical Engineering, Konkuk University, Seoul 05029, Republic of Korea*

Author contributions

S.H. and S.W.B. designed the study, analysed the data, and wrote the manuscript. S.H. performed most experiments and S.S. supported BPM electrolyzer fabrication and measurements. M.S. performed AFM measurements. Y.W. collected TEM data. O.T.V. supported QCM measurement and fabrication of 100 cm^2 WD catalyst. S. Hou supported the fabrication of the ED-Co anode catalyst. S.K. and J.Y.L. synthesized HQPC-TMA membranes and conducted in-plane conductivity measurements. J.Y. and S.W.B. supervised the project. All authors participated in and contributed to the final version.

Notes

The authors declare no competing interests.

ACKNOWLEDGMENT

The studies of the effect of catalyst structure on ionic and reaction water dissociation resistances in the BPM and the BPM electrolyzer testing was supported by the US Office of Naval Research (grant N00014-23-1-2820 and N00014-24-1-2433). The scale-up efforts for the BPM were funded by the National Science Foundation Partnerships for Innovation program Award #2141201. This work was also supported by the National Research Foundation of Korea (NRF) grant funded by the Korea government (MSIT) (RS-2024-00348577) and the joint international research grant program (2024) scholarship from BK21 FOUR Graduate School Innovation Center in Seoul National University (SNU). We acknowledge the use of shared instrumentation in the Center for Advanced Materials Characterization in Oregon (CAMCOR). We appreciate the staff of the University of California Berkeley Electron Microscope Laboratory for advice and assistance in electron microscopy sample preparation and data collection.

REFERENCES

(1) Rodellar, C. G.; Gisbert-Gonzalez, J. M.; Sarabia, F.; Roldan Cuenya, B.; Oener, S. Z. Ion Solvation Kinetics in Bipolar Membranes and at Electrolyte–Metal Interfaces. *Nat. Energy* **2024**, *9*, 548–558. https://doi.org/10.1038/s41560-024-01484-z.

(2) Toh, W. L.; Dinh, H. Q.; Chu, A. T.; Sauvé, E. R.; Surendranath, Y. The Role of Ionic Blockades in Controlling the Efficiency of Energy Recovery in Forward Bias Bipolar Membranes. *Nat. Energy* **2023**, *8* (12), 1405–1416. https://doi.org/10.1038/s41560-023-01404-7.

(3) Oener, S. Z.; Foster, M. J.; Boettcher, S. W. Accelerating Water Dissociation in Bipolar Membranes and for Electrocatalysis. *Science (80).* **2020**, *369* (6507), 1099–1103. https://doi.org/10.1126/science.aaz1487.

(4) Bui, J. C.; Lees, E. W.; Marin, D. H.; Stovall, T. N.; Chen, L.; Kusoglu, A.; Nielander, A. C.; Jaramillo, T. F.; Boettcher, S. W.; Bell, A. T.; Weber, A. Z. Multi-Scale Physics of Bipolar Membranes in Electrochemical Processes. *Nat. Chem. Eng.* **2024**, *1* (1), 45–60. https://doi.org/10.1038/s44286-023-00009-x.

(5) Marin, D. H.; Perryman, J. T.; Hubert, M. A.; Lindquist, G. A.; Chen, L.; Aleman, A. M.; Kamat, G. A.; Niemann, V. A.; Stevens, M. B.; Regmi, Y. N.; Boettcher, S. W.; Nielander, A. C.; Jaramillo, T. F. Hydrogen Production with Seawater-Resilient Bipolar Membrane Electrolyzers. *Joule* **2023**, *7* (4), 765–781. https://doi.org/10.1016/j.joule.2023.03.005.

(6) Öner, M. R.; Kanca, A.; Ata, O. N.; Yapici, S.; Yaylali, N. A. Bipolar Membrane Electrodialysis for Mixed Salt Water Treatment: Evaluation of Parameters on Process Performance. *J. Environ. Chem. Eng.* **2021**, *9* (4), 105750. https://doi.org/10.1016/j.jece.2021.105750.

(7) Han, S.; Jeon, S. il; Lee, J.; Ahn, J.; Lee, C.; Lee, J.; Yoon, J. Efficient Bicarbonate Removal and Recovery of Ammonium Bicarbonate as CO2 Utilization Using Flow-Electrode Capacitive Deionization. *Chem. Eng. J.* **2022**, *431*, 134233. https://doi.org/10.1016/j.cej.2021.134233.

(8) Suss, M. E.; Porada, S.; Sun, X.; Biesheuvel, P. M.; Yoon, J.; Presser, V. Water Desalination via Capacitive Deionization: What Is It and What Can We Expect from It? *Energy Environ. Sci.* **2015**, *8* (8), 2296–2319. https://doi.org/10.1039/c5ee00519a.

(9) Arana Juve, J. M.; Christensen, F. M. S.; Wang, Y.; Wei, Z. Electrodialysis for Metal Removal and Recovery: A Review. *Chem. Eng. J.* **2022**, *435* (P2), 134857. https://doi.org/10.1016/j.cej.2022.134857.

(10) Thiele, S.; Mayerhöfer, B.; McLaughlin, D.; Böhm, T.; Hegelheimer, M.; Seeberger, D. Bipolar Membrane Electrode Assemblies for Water Electrolysis. *ACS Appl. Energy Mater.* **2020**, *3* (10), 9635–9644. https://doi.org/10.1021/acsaem.0c01127.

(11) Faqeeh, A. H.; Symes, M. D. Zero-Gap Bipolar Membrane Water Electrolyzers: Principles, Challenges and Practical Insights. *Electrochim. Acta* **2024**, *493* (January), 144345. https://doi.org/10.1016/j.electacta.2024.144345.

(12) Hong, E.; Yang, Z.; Zeng, H.; Gao, L.; Yang, C. Recent Development and Challenges of Bipolar Membranes for High Performance Water Electrolysis. *ACS Mater. Lett.* **2024**, *6*, 1623–1648. https://doi.org/10.1021/acsmaterialslett.3c01227.

(13) Chen, L.; Xu, Q.; Oener, S. Z.; Fabrizio, K.; Boettcher, S. W. Design Principles for Water Dissociation Catalysts in High-Performance Bipolar Membranes. *Nat. Commun.* **2022**, *13* (1), 3846. https://doi.org/10.1038/s41467-022-31429-7.

(14) Chen, L.; Xu, Q.; Boettcher, S. W. Kinetics and Mechanism of Heterogeneous Voltage-Driven Water-Dissociation Catalysis. *Joule* **2023**, *7* (8), 1867–1886. https://doi.org/10.1016/j.joule.2023.06.011.

(15) Petrov, K. V.; Koopman, C. I.; Subramanian, S.; Koper, M. T. M.; Burdyny, T.; Vermaas, D. A. Bipolar Membranes for Intrinsically Stable and Scalable CO2 Electrolysis. *Nat. Energy* **2024**, *9* (August), 932–938. https://doi.org/10.1038/s41560-024-01574-y.

(16) Hu, L.; Wrubel, J. A.; Baez-Cotto, C. M.; Intia, F.; Park, J. H.; Kropf, A. J.; Kariuki, N.; Huang, Z.; Farghaly, A.; Amichi, L.; Saha, P.; Tao, L.; Cullen, D. A.; Myers, D. J.; Ferrandon, M. S.; Neyerlin, K. C. A Scalable Membrane Electrode Assembly Architecture for Efficient Electrochemical Conversion of CO2 to Formic Acid. *Nat. Commun.* **2023**, *14* (1), 7605. https://doi.org/10.1038/s41467-023-43409-6.

(17) Disch, J.; Ingenhoven, S.; Vierrath, S. Bipolar Membrane with Porous Anion Exchange Layer for Efficient and Long-Term Stable Electrochemical Reduction of CO2 to CO. *Adv. Energy Mater.* **2023**, *13* (38), 2301614. https://doi.org/10.1002/aenm.202301614.

(18) Ünlü, M.; Zhou, J.; Kohl, P. A. Hybrid Anion and Proton Exchange Membrane Fuel Cells. *J. Phys. Chem. C* **2009**, *113* (26), 11416–11423. https://doi.org/10.1021/jp903252u.
(19) Zhu, P.; Wu, Z. Y.; Elgazzar, A.; Dong, C.; Wi, T. U.; Chen, F. Y.; Xia, Y.; Feng, Y.; Shakouri, M.; Kim, J. Y. (Timothy); Fang, Z.; Hatton, T. A.; Wang, H. Continuous Carbon Capture in an Electrochemical Solid-Electrolyte Reactor. *Nature* **2023**, *618* (7967), 959–966. https://doi.org/10.1038/s41586-023-06060-1.
(20) Bui, J. C.; Lucas, É.; Lees, E. W.; Liu, A. K.; Atwater, H. A.; Xiang, C.; Bell, A. T.; Weber, A. Z. Analysis of Bipolar Membranes for Electrochemical CO2 Capture from Air and Oceanwater. *Energy Environ. Sci.* **2023**, *16* (11), 5076–5095. https://doi.org/10.1039/d3ee01606d.
(21) Oener, S. Z.; Twight, L. P.; Lindquist, G. A.; Boettcher, S. W. Thin Cation-Exchange Layers Enable High-Current-Density Bipolar Membrane Electrolyzers via Improved Water Transport. *ACS Energy Lett.* **2021**, *6* (1), 1–8. https://doi.org/10.1021/acsenergylett.0c02078.
(22) Li, J.; Morthensen, S. T.; Zhu, J.; Yuan, S.; Wang, J.; Volodine, A.; Lin, J.; Shen, J.; Van der Bruggen, B. Exfoliated MoS2 Nanosheets Loaded on Bipolar Exchange Membranes Interfaces as Advanced Catalysts for Water Dissociation. *Sep. Purif. Technol.* **2018**, *194* (June 2017), 416–424. https://doi.org/10.1016/j.seppur.2017.11.065.
(23) Kovtyukhova, N. I.; Ollivier, P. J.; Martin, B. R.; Mallouk, T. E.; Buzaneva, E. V.; Gorchinskiy, A. D. Layer-by-Layer Assembly of Ultrathin Composite Films from Micron-Sized Graphite Oxide Sheets and Polycations. *Chem. Mater.* **1999**, *11* (3), 771–778. https://doi.org/10.1021/cm981085u.
(24) Chen, Y.; Wrubel, J. A.; Klein, W. E.; Kabir, S.; Smith, W. A.; Neyerlin, K. C.; Deutsch, T. G. High-Performance Bipolar Membrane Development for Improved Water Dissociation. *ACS Appl. Polym. Mater.* **2020**, *2* (11), 4559–4569. https://doi.org/10.1021/acsapm.0c00653.
(25) Sasmal, S.; Chen, L.; Sarma, P. V; Vulpin, O. T.; Simons, C. R.; Wells, K. M.; Spontak, R. J.; Boettcher, S. W. Materials Descriptors for Advanced Water Dissociation Catalysts in Bipolar Membranes. *Nat. Mater.* **2024**, *23*, 1421–1427. https://doi.org/10.1038/s41563-024-01943-8.
(26) Xiao, J.; Oliveira, A. M.; Wang, L.; Zhao, Y.; Wang, T.; Wang, J.; Setzler, B. P.; Yan, Y. Water-Fed Hydroxide Exchange Membrane Electrolyzer Enabled by a Fluoride-Incorporated Nickel-Iron Oxyhydroxide Oxygen Evolution Electrode. *ACS Catal.* **2021**, *11* (1), 264–270. https://doi.org/10.1021/acscatal.0c04200.
(27) Kwak, M.; Ojha, K.; Shen, M.; Boettcher, S. W. Electrically Insulated Catalyst–Ionomer Anode Interfaces toward Durable Alkaline Membrane Electrolyzers. *ACS Energy Lett.* **2024**, *9*, 1025–1034. https://doi.org/10.1021/acsenergylett.3c02620.
(28) Lindquist, G. A.; Oener, S. Z.; Krivina, R.; Motz, A. R.; Keane, A.; Capuano, C.; Ayers, K. E.; Boettcher, S. W. Performance and Durability of Pure-Water-Fed Anion Exchange Membrane Electrolyzers Using Baseline Materials and Operation. *ACS Appl. Mater. Interfaces* **2021**, *13* (44), 51917–51924. https://doi.org/10.1021/acsami.1c06053.
(29) Kim, S.; Yang, S. H.; Shin, S. H.; Cho, H. J.; Jang, J. K.; Kim, T. H.; Oh, S. G.; Kim, T. H.; Han, H. S.; Lee, J. Y. High-Performance and Durable Anion-Exchange Membrane Water Electrolysers with High-Molecular-Weight Polycarbazole-Based Anion-Conducting Polymer. *Energy Environ. Sci.* **2024**, *17*, 5399–5409. https://doi.org/10.1039/d4ee01003e.

(30) Han, S.; Ryu, J. H.; Lee, W. B.; Ryu, J.; Yoon, J. Translating the Optimized Durability of Co-Based Anode Catalyst into Sustainable Anion Exchange Membrane Water Electrolysis. *Small* **2024**, *20* (27), 2311052. https://doi.org/10.1002/smll.202311052.
(31) Han, S.; Park, J.; Yoon, J. Surface Reconstruction of Co-Based Catalysts for Enhanced Oxygen Evolution Activity in Anion Exchange Membrane Water Electrolysis. *Adv. Funct. Mater.* **2024**, *34* (21), 2314573. https://doi.org/10.1002/adfm.202314573.
(32) Han, S.; Park, H. S.; Yoon, J. Superior Performance of an Anion Exchange Membrane Water Electrolyzer: Sequential Electrodeposited Co-Based Oxygen Evolution Catalyst. *Chem. Eng. J.* **2023**, *477*, 146713. https://doi.org/10.1016/j.cej.2023.146713.
(33) Electrocatalysts, G.; Zheng, Y.; Serban, A.; Zhang, H.; Chen, N.; Song, F.; Hu, X. Anion Exchange Ionomers Enable Sustained Pure-Water Electrolysis Using Platinum-Group-Metal-Free Electrocatalysts. *ACS Energy Lett.* **2023**, *8*, 5018–5024. https://doi.org/10.1021/acsenergylett.3c01866.
(34) Sheng, W.; Zhuang, Z.; Gao, M.; Zheng, J.; Chen, J. G.; Yan, Y. Correlating Hydrogen Oxidation and Evolution Activity on Platinum at Different PH with Measured Hydrogen Binding Energy. *Nat. Commun.* **2015**, *6*, 6–11. https://doi.org/10.1038/ncomms6848.
(35) Vulpin, O. T.; Mitchell, J. B.; Chen, L.; Lim, J.; Sasmal, S.; Price, N. G.; Jarvis, S. R.; Boettcher, S. W. Comparing Advanced Bipolar Membranes for High-Current Electrodialysis and Membrane Electrolysis. *ACS Energy Lett.* **2025**, *10*, 845–852. https://doi.org/10.1021/acsenergylett.4c03538.
(36) Krivina, R. A.; Lindquist, G. A.; Beaudoin, S. R.; Stovall, T. N.; Thompson, W. L.; Twight, L. P.; Marsh, D.; Grzyb, J.; Fabrizio, K.; Hutchison, J. E.; Boettcher, S. W. Anode Catalysts in Anion-Exchange-Membrane Electrolysis without Supporting Electrolyte: Conductivity, Dynamics, and Ionomer Degradation. *Adv. Mater.* **2022**, *34* (35), 2203033. https://doi.org/10.1002/adma.202203033.
(37) Lindquist, G. A.; Gaitor, J. C.; Thompson, W. L.; Brogden, V.; Noonan, K. J. T.; Boettcher, S. W. Oxidative Instability of Ionomers in Hydroxide-Exchange-Membrane Water Electrolyzers. *Energy Environ. Sci.* **2023**, *16* (10), 4373–4387. https://doi.org/10.1039/d3ee01293j.
(38) Haghighi, M.; Ghazyani, N.; Mahmoodpour, S.; Keshtmand, R.; Ghaffari, A.; Luo, H.; Mohammadpour, R.; Taghavinia, N.; Abdi-Jalebi, M. Low-Temperature Processing Methods for Tin Oxide as Electron Transporting Layer in Scalable Perovskite Solar Cells. *Solar PRL.* **2023**, 7, 2201080. https://doi.org/10.1002/solr.202201080.
(39) Garbe, S.; Futter, J.; Agarwal, A.; Tarik, M.; Mularczyk, A. A.; Schmidt, T. J.; Gubler, L. Understanding Degradation Effects of Elevated Temperature Operating Conditions in Polymer Electrolyte Water Electrolyzers. *J. Electrochem. Soc.* **2021**, *168* (4), 044515. https://doi.org/10.1149/1945-7111/abf4ae.
(40) Osborn, S. J.; Hassan, M. K.; Divoux, G. M.; Rhoades, D. W.; Mauritz, K. A.; Moore, R. B. Glass Transition Temperature of Perfluorosulfonic Acid Ionomers. *Macromolecules* **2007**, *40* (10), 3886–3890. https://doi.org/10.1021/ma062029e.
(41) Shaik, S.; Kundu, J.; Yuan, Y.; Chung, W.; Han, D.; Lee, U.; Huang, H.; Choi, S. Il. Recent Progress and Perspective in Pure Water-Fed Anion Exchange Membrane Water Electrolyzers. *Adv. Energy Mater.* **2024**, *35*, 2401956. https://doi.org/10.1002/aenm.202401956.
(42) Lim, J.; Klein, J. M.; Lee, S. G.; Park, E. J.; Kang, S. Y.; Maurya, S.; Mustain, W. E.; Boettcher, S.; Kim, Y. S. Addressing the Challenge of Electrochemical Ionomer Oxidation in Future Anion Exchange Membrane Water Electrolyzers. *ACS Energy Lett.* **2024**, *9* (6), 3074–3083. https://doi.org/10.1021/acsenergylett.4c00832.
(43) Mayerhöfer, B.; Speck, F. D.; Hegelheimer, M.; Bierling, M.; Abbas, D.; McLaughlin, D.; Cherevko, S.; Thiele, S.; Peach, R. Electrochemical- and Mechanical Stability of

Catalyst Layers in Anion Exchange Membrane Water Electrolysis. *Int. J. Hydrogen Energy* **2022**, *47* (7), 4304–4314. https://doi.org/10.1016/j.ijhydene.2021.11.083.

(44) Wan, L.; Liu, J.; Xu, Z.; Xu, Q.; Pang, M.; Wang, P.; Wang, B. Construction of Integrated Electrodes with Transport Highways for Pure-Water-Fed Anion Exchange Membrane Water Electrolysis. *Small* **2022**, *18* (21), 2200380. https://doi.org/10.1002/smll.202200380.

TOC Graphic